Mitochondrial Peptides Target, but do not Denature Soluble Amyloids in Type II Diabetes

Zachary A. Levine,[1,2,*] Kazuki Teranishi,[3,4] Alan K. Okada,[3,4,§]
Ralf Langen,[3,4] and Joan-Emma Shea[5,6]

1. Department of Pathology
   Yale School of Medicine, New Haven, CT, 06520, USA

2. Department of Molecular Biophysics & Biochemistry,
   Yale University, New Haven, CT 06520, USA

3. Department of Biochemistry and Molecular Biology
   University of Southern California, Los Angeles, CA 90033, USA

4. Zilkha Neurogenetic Institute, Keck School of Medicine
   University of Southern California, Los Angeles, CA 90033, USA

5. Department of Chemistry and Biochemistry,
   University of California Santa Barbara, Santa Barbara, CA 93106, USA

6. Department of Physics,
   University of California Santa Barbara, Santa Barbara, CA 93106, USA

§ Present Address:

Department of Emergency Medicine
Regions Hospital, St. Paul, MN 55101, USA

*** Corresponding author:**

Zachary A. Levine
Department of Pathology
Department of Molecular Biophysics & Biochemistry
Yale University, New Haven, CT 06520, USA
Email: zachary.levine@yale.edu

ABSTRACT

Mitochondrially-derived peptides (MDPs) such as humanin (HN) have shown a remarkable ability to modulate neurological amyloids and apoptosis-associated proteins in cells and animal models. Recently, we found that humanin-like peptides also inhibit amyloid formation outside of neural environments in islet amyloid polypeptide (IAPP) fibrils and plaques, which are hallmarks of Type II Diabetes. However, the biochemical basis for regulating amyloids through endogenous MDPs remains elusive. One hypothesis is that MDPs stabilize intermediate amyloid oligomers and discourage the formation of insoluble fibrils. In order to test this hypothesis, we carried out simulations and experiments to extract the dominant interactions between the S14G-HN mutant (HNG) and a diverse set of IAPP structures. Replica-exchange molecular dynamics suggests that MDPs cap the growth of amyloid oligomers. Simulations also indicate that HNG-IAPP heterodimers are ten times more stable than IAPP homodimers, which explains the sub-stoichiometric ability of HNG to inhibit amyloid growth. Despite this strong attraction, HNG does not denature IAPP. Instead, HNG binds IAPP near the disordered NFGAIL motif, wedging itself between amyloidogenic fragments. Shielding of NFGAIL-flanking fragments reduces the formation of parallel IAPP β-sheets and subsequent nucleation of mature amyloid fibrils. From ThT spectroscopy and electron microscopy, we found that HNG does not deconstruct mature IAPP fibrils and oligomers, consistent with the simulations and our proposed hypothesis. Taken together, this work provides new mechanistic insight into how endogenous MDPs regulate pathological amyloid growth at the molecular level and in highly substoichiometric quantities, which can be exploited through peptidomimetics in Diabetes or Alzheimer's Disease.

KEYWORDS

Type II Diabetes, Humanin, S14G, IAPP, Amylin, Protein Folding, Molecular Dynamics Simulations, Replica-Exchange Molecular Dynamics, Umbrella Sampling, Intrinsically Disordered Proteins, Amyloid, Amyloid Fibrils, Soluble Oligomers.

INTRODUCTION

Nearly every eukaryotic cell relies on the mitochondria, a small granular organelle, to synthesize the molecules necessary for intracellular energy transfer. The origins of modern mitochondria are believed to originate from bacteria[1] that symbiotically merged with eukaryotic cells sometime between one to two billion years ago, carrying with them a partially conserved genome that has persisted in parallel alongside the nuclear genome.[2] The interiors of mitochondria are tightly packed into cristae and encapsulated by dual phospholipid membranes, with an inner matrix rich in enzymes, ribosomes, and proteins that are unique to the organelle. Some of these proteins are dually coded in the mitochondrial and nuclear genomes,[3] however mitochondrial proteins tend to be optimized to function in confined spaces and may carry out unique functions outside their natural environments.[4] It is thus unclear what roles mitochondrial peptides play in the cytosol, if any, or if their functions are conserved from inside the tightly packed organelle to the relatively expansive cellular interior.

While the mitochondrial genome was fully sequenced in 1981,[5] it took twenty years for the first novel mitochondrial peptides to be identified in 2001[6] from three independent studies focusing on apoptosis signaling,[7] insulin-like growth factors in the context of aging,[8] and neurodegenerative plaques associated with Alzheimer's Disease.[6] The first peptide to be identified, humanin (HN), was found in the 16s ribosomal subunit of the mitochondrial genome and is composed of either 21 or 24 amino acids when expressed in the mitochondria or cytosol, respectively (seq: MAPRGFSCLLLLTSEIDLPVKRRA). Given the relatively small size of HN, its ability to modulate a wide variety of physiological processes is remarkable, with pronounced effects on yeast models,[8] rats,[9] mice,[10] and humans.[11] Furthermore, the potency of HN can be amplified through a number of post-translational modifications, as observed in HN-S14G (or HNG, where Ser14 is replaced by a glycine residue), which has consistently been shown to be neuro- and cyto-protective in animal models.[12-13] However, the molecular mechanisms behind HN and HNG-mediated cytoprotection are unclear, and are difficult to experimentally identify since regions of the peptide are intrinsically disordered, aside from a characteristic α-helix found near the hydrophobic center.

Recently, we reported that HNG also inhibits the fibrilization of islet amyloid polypeptide[14] (or IAPP, seq: KCNTATCATQRLANFLVHSSNNFGAILSSTNVGSNTY). IAPP is an intrinsically disordered amyloid protein (IDP) that is co-expressed with insulin in pancreatic β-cells. During the overexpression of insulin in Type II Diabetes, large amounts of IAPP are also released, leading to the pathological accumulation of amyloid fibrils on β-cell surfaces that rupture protective membranes[15-18] and encourage pancreatic dysfunction. Given that Type II Diabetes comprises 90% of all Diabetes cases worldwide,[19] affecting over 350 million individuals, it is imperative to understand how endogenous IDPs such as those found in the mitochondria can affect or even regulate pathological amyloid precursors. In the case of IAPP, some have suggested that pathological aggregation is nucleated by its disordered NFGAIL region,[20-24] which acts as a linker

between β-stranded regions. Others have argued that serine-rich flanking amino acids around NFGAIL are the primary drivers of aggregation.[25] In order to deduce the biochemical interactions between pathological IAPP oligomers and HNG, we have integrated multiscale theoretical models with experimental observations in order to provide a robust picture of humanin's role in inhibiting pathological amyloids from first principles. These methods allow us to test our working hypothesis that HNG inhibits IAPP amyloid growth[14, 26] through the capping of oligomeric amyloid seeds using synergistic and systematic *de-novo* studies.

To better understand these molecular interactions, atomistic molecular dynamics (MD) simulations were employed to investigate the folding and oligomerization of IAPP in the presence of HNG. In particular, replica-exchange MD (REMD)[27] was used to reveal the accessible thermodynamic landscapes each protein inhabits in isolation and in the presence of one another. A wide variety of degenerate protein structures occupying low-energy basins were extracted from these ensembles in an effort to learn what secondary structures drive HNG-IAPP complexation. Simulations were also able to differentiate monomeric, oligomeric, and fibrillar interactions in order to provide multiscale models of HNG-IAPP assemblies. In order to characterize the strength of adhesion between homo- and heterodimer structures, umbrella sampling simulations[28] were carried out and free energies of adhesion are reported. These results are all consistent with our previous ThT spectroscopy, electron microscopy (EM), circular dichroism (CD), and electron paramagnetic resonance (EPR) results,[14] which corroborates the molecular observations reported here. We also provide specific molecular pathways that drive MDP-mediated inhibition of IAPP aggregation, supported by new experimental results on mature IAPP fibrils. Given the broad efficacy of HNG in reducing pathological aggregation across a wide variety of amyloids,[13] we briefly discuss the versatility of MDPs in regulating misfolding and aggregation of generalized amyloid proteins.[29] As a result, we believe that our results can inform MDP-inspired therapeutics that target soluble amyloid pharmacophores rather than traditional compounds that seek to destabilize and clear mature fibrils and plaques.

RESULTS

First, we will describe backbone conformations from each complex resulting from enhanced-sampling MD simulations. REMD reveals a wide variety of monomeric, homodimeric, heterodimeric, and trimeric protein conformations for HNG and IAPP mixtures, however the most populous structures (ranked by their occupation times) are presented in Figure 1. As expected, HNG monomers and dimers preserved their central α-helix while the remaining residues remain disordered, however HNG tended to adopt compact globular morphologies both in isolation and when oligomerized. Alternatively, while IAPP monomers remained largely disordered in bulk solution (sometimes sampling partial β-strands), they adopted highly ordered β-strands and hairpins when coupled to a neighboring IAPP or HNG monomer in both parallel and anti-parallel geometries. This behavior is expected from IAPP, as it is an intrinsically disordered monomer that is stabilized during oligomerization, where the formation of uniform β-sheets helps to seed further aggregation.[30-34] In heterodimer mixtures, each protein adopts a similar conformation to their homodimeric state. However, HNG predominantly binds to the side of IAPP hairpins in heterodimers and trimers, similar to where aggregating IAPP would attach. Interestingly in heterotrimers, HNG is either wedged between IAPP hairpins or offsets and unzips IAPP dimers in order to maximize hydrophobic contact with IAPP. Such interactions would assuredly affect the growth and uniformity of higher order amyloid structures.

The relative time spent in these states are short compared to globular proteins, though these fractions are consistent with other IDPs.[29, 35-36] A useful way to visualize the interconversion between states is to construct conformational free energy landscapes (or FELs) that highlight protein ensembles as a function of multiple parameters. Two useful order parameters for characterizing IDPs are the protein end-to-end distance (R_{ee}) and the radius of gyration (R_g), which can be coupled together to differentiate compact and extended IDP morphologies.[29] Here (Figure S1), FELs reveal that both HNG and IAPP monomers easily interconvert between compact (small R_{ee} and R_g) and extended (large R_{ee} and R_g) morphologies. However, when IAPP dimerizes its preferred radius of gyration increases while its end-to-end-distance remains unchanged. These shifts are a hallmark of β-hairpin formation, and also occur when IAPP binds to HNG. In contrast, FELs for HNG do not significantly shift in the presence of IAPP, though its end-to-end distance stabilizes in crowded environments to 2-3 nm. Overall, the FELs for HNG and IAPP are similar before and after complexation occurs, suggesting that the two proteins do not significant denature the backbones of their binding partners.

Heterodimer mixtures also do not exhibit new secondary structures compared to homodimers, suggesting that HNG does not induce fundamentally new IAPP structures (Figure 2). However, the introduction of additional HNG or IAPP is associated with a marginal increase in IAPP β-content. It is unclear from REMD whether HNG directly stabilizes IAPP monomers after binding or simply binds to IAPP after it samples a transient β-hairpin conformation. While the magnitude of IAPP aggregation was significantly reduced in previous experiments with HNG present,[14] the

kinetic timescales of complexation were similar in ThT spectroscopy. If HNG immediately stabilized monomeric IAPP, then the kinetic timescales of complexation should differ,[37-39] even with substoichiometric amounts of HNG. Thus, it is more likely that HNG binds to IAPP only after β-strands begin to stabilize, consistent with our hypothesis that HNG targets intermediate or soluble IAPP oligomers. IAPP β-content continues to increase as additional IAPP or HNG are added, while α-content (dominated primarily by the disulfide near the N-terminus) remains minimal. IAPP also does not significantly shift the secondary structures of HNG (Figure S2), however small HNG secondary structures become stabilized during crowding, especially the helix-turn-bend motif. This is similar to existing NMR studies that show that HN is stabilized in the presence of 30% tetrafluoroethylene.[40]

While HNG and IAPP did not significantly denature one another, HNG did modify the relative orientation between IAPP monomers, which is shown in Figure 3. Consistent with the most dominant protein states, thermodynamic FELs were extracted as a function of relative IAPP orientation and separation. When HNG was absent, IAPP dimers were spaced about 1 nm apart and tended to be arranged in parallel β-strands. However, when HNG was introduced, IAPP was forced to adopt anti-parallel β-sheets that were much less stable than their parallel counterparts. Some parallel IAPP states persisted, but in those cases IAPP was separated by 2 nm instead of 1 nm, which resulted in less stable complexes. Taken together with Figure 1, HNG effectively separates, unzips, or offsets IAPP dimers from adopting their most energy-minimized conformations, consistent with our previous data[14] showing that HNG potently inhibits IAPP aggregation.

In order to test if specific regions drive these interactions, we focus on both the HNG Gly14 residue (mutated from serine) and the IAPP NFGAIL region, which has long been linked to pathological aggregation in Type II Diabetes. [20, 39, 41] REMD simulations reveal that when IAPP oligomers form, there is considerable association between NFGAIL regions (Figure S3, yellow). However, when HNG is introduced, NFGAIL and its serine-rich flanking domains (SN-NFGAIL-SS) remain separated by both direct (screening) and indirect (out-of-register) interactions, which have pronounced effects on the oligomer's geometry. Conversely, HNG Gly14 contributes very minimally towards folding and aggregation, despite its presence differentiating wt from mutant IAPP. We hypothesize that the removal of the wildtype serine imparts additional conformational flexibility to HNG, further allowing it to conform to hydrophobic IAPP interfaces.

Specific protein-protein interactions such as salt-bridge formation and backbone hydrogen bonding also appears to modulate the types of HNG:IAPP mixtures that were formed (Figures S4 and S5). Each polar residue on IAPP is positively charged, so all dominant electrostatic interactions between oppositely-charged side-chains stem from HNG. Intramolecular HNG salt bridges tend to form between C-terminal Arg residues and nearby Asp or Glu. However, there are few intermolecular salt bridges between HNG and IAPP interfaces in heterodimers and mixed trimers. Instead, HNG:IAPP mixtures are stabilized by a combination of intra- and intermolecular

backbone hydrogen bonds (Figure S5), with IAPP monomers and dimers exhibiting 9-13 intramolecular bonds (0.25-0.35 bonds per residue) versus HNG monomers and dimers that exhibit about 5 intramolecular bonds (0.20 bonds per residue). Some of the IAPP intramolecular hydrogen bonds are converted into intermolecular bonds upon mixing, which maximizes protein hydrophobicity for HNG on the side of IAPP β-hairpins. In trimers, HNG occupies one to two externally-facing hydrogen bonds from IAPP, thus reducing the number of available sites for subsequent IAPP to hydrogen bond to. This suggests that HNG binds most favorably to unbound or metastable IAPP proteins while they adopt hairpin conformations, which supports the hypothesis that HNG targets and screens interfacial IAPP proteins that seed aggregation.

In order to more explicitly investigate the adhesion between HNG and IAPP proteins, potentials of mean force were extracted from umbrella sampling simulations[42] to measure the free energy of IAPP binding between dominant homodimers, heterodimers, and trimers. These results, plotted in Figure 4, indicate that IAPP dimers are strongly bound by 7.5 ± 2.6 kT of energy, and are stabilized by interactions between complementary β-hairpins. Quite dramatically, however, mixed HNG:IAPP heterodimers are stabilized by 100 ± 3 kT (or nearly 10-13 times the binding affinity of IAPP homodimers). The contrast between homodimer and heterodimer adhesion is striking, and suggests a significant attraction between HNG and IAPP, even in the presence of multiple IAPP proteins. It should be noted, however, that heterodimer adhesion profiles were measured between a disordered HNG and a highly ordered IAPP hairpin, since this represents the most energetically favorable heterodimer cluster identified in Figure 1. As indicated earlier, this data suggests that HNG is strongly attracted to oligomeric IAPP, which we define as a free or loosely bound β-hairpin structure. Since few interactions from REMD were observed between disordered IAPP monomers and HNG, interactions between natively disordered monomers are likely smaller or non-existent, consistent with experiments.[14] IAPP also adheres to HNG-IAPP dimers (in a trimeric conformation) more strongly than to IAPP monomers (in a dimer conformation) at 10.6 ± 2.5 kT, which is due to the presence of bound HNG inside the attracting dimer. While β-hairpin IAPP is strongly attracted to HNG monomers, subsequent IAPP attachment becomes continually less favorable due to screening of the internal HNG molecule. As a result, mixed trimers are more energetically stable than IAPP dimers, though in larger oligomers, the adhesion strength should approach that of the dimer, since HNG will eventually be screened entirely. These observations further support the hypothesis that sub-stoichiometric HNG caps IAPP oligomers, as others have postulated, and may function as a chaperonin.[14, 26]

Protein contact maps (Figure S6) were also used to identify interactions between non-polar amino acids within ensembles, and to highlight associations between distinct regions of HNG and IAPP. Since IAPP and HNG monomers are predominantly disordered, very few persistent intramolecular contacts were identified in monomeric structures. However, homo- and heterodimer contact maps revealed characteristic α-helical signatures in HNG and β-stranded signatures in IAPP, consistent with Figure 1. In terms of intermolecular contacts, IAPP homodimers (consisting of parallel and anti-parallel β-hairpins) are distinct from those found in HNG-containing trimers, where there is

significantly less contact between IAPP termini. For mixed HNG:IAPP systems, there is persistent contact between HNG-$_{9}$LLLL$_{12}$ (a bend-turn region) and IAPP-$_{11}$RLA$_{13}$ or IAPP-$_{26}$ILS$_{28}$ (β-strand regions). There is also contact between HNG-$_{20}$VKR$_{22}$ (a polar region) and IAPP-$_{13}$ANF$_{15}$ or IAPP-$_{25}$AIL$_{27}$ (β-strand regions). Many of these IAPP regions include or flank the $_{12}$LANFLV$_{17}$ and $_{22}$NFGAIL$_{27}$ regions, lying at the interface between disordered and β-stranded backbones. The IAPP-$_{20}$SNNFGAILSS$_{29}$ region, in particular, is strongly aggregation-prone[39] and transitions IAPP β-strands into disordered linker loops, as can be seen in Figure 2.

In order to investigate the putative binding locations of HNG monomers to larger IAPP fibrils, two additional MD simulations were run on an HNG monomer and two distinct IAPP fibril geometries. Each fibril structure contained ten monomers, and were based on previously reported structures from EPR and NMR.[34, 43] In these simulations, which lasted 100 ns, HNG quickly attaches to each fibril exterior spanning multiple IAPP monomers, and remains bound for a majority of the simulation (~30-100 ns). Interactions with each fibril structure, shown in Figure 5, confirm that HNG associates with and binds to NFGAIL-flanking motifs. This suggests that HNG seeks to maximize contact with as many NFGAIL-associated regions as possible and align its crowd-stabilized β-bend with the IAPP β-strand region. Neither the HNG monomers nor IAPP fibrils became denatured during their interaction, consistent with the REMD simulations reported earlier. Similarly, conserved interactions between HNG and two distinct IAPP fibrils reduces the likelihood that specific fibrillar geometries favor interactions with HNG, so long as the SS and SN flanking regions around NFGAIL are solvent-exposed.

We also investigated whether HNG could deconstruct mature amyloid fibrils in experiments, in addition to slowing or halting the nucleation of new IAPP fibers. Similar to our earlier experiments,[14] we confirmed that HNG potently inhibited the formation of insoluble IAPP fibrils using electron microscopy and Thioflavin T (ThT) spectroscopy. We also found that HNG counteracted the growth of new IAPP fibrils from preformed IAPP seeds.[14] Using similar conditions, we tested whether the addition of HNG reduces ThT fluorescence over time in IAPP fibrils, indicating a loss of protein β-content. As a positive control for fibril dissolution, we used 4 M guanidinium chloride, which is a potent protein denaturant capable of deconstructing amyloid fibrils. As illustrated in Figure 6, the addition of HNG did not alter ThT fluorescence significantly over 24 hours. In contrast, the addition of guanidinium quickly led to a decrease in ThT fluorescence. This indicates that HNG does not appreciably dissolve IAPP fibrils. To better visualize these fibrillar morphologies under each condition, we performed electron microscopy on negatively stained samples. As shown in Figure 6, IAPP fibrils exhibit the typical, often bundled morphology that remains unaffected by the addition of HNG. In contrast, the addition of guanidinium reduces the prevalence of fibrils significantly while only few aggregates, often very short, remain. These results indicate that HNG blocks the nucleation of IAPP aggregates but does not dissolve them in any detectable amount.

DISCUSSION

Taken together, our observations corroborate the hypothesis that HNG targets oligomeric IAPP and subsequently inhibits its ability to aggregate. Simulations suggest that HNG binding to exposed NFGAIL motifs during IAPP oligomerization mediates this behavior through the offset of IAPP hydrogen-bond networks that nucleate the formation of fibrils, consistent with our earlier ThT, CD, and EPR experiments.[14] Molecular models are also consistent with our observations of sub-stoichiometric amounts of HNG inhibiting both primary (fiber-independent) and secondary (fiber-dependent) IAPP aggregation from monomers and sonicated seeds. Given the substantial effect of HNG in miniscule concentrations (three orders of magnitude below IAPP),[14] a cap-and-contain mechanism[26] appears to be the most likely explanation for this behavior, especially in the absence of a HNG-induced denaturing cascade. Other endogenous molecules, such as insulin, can also block IAPP oligomerization in stoichiometric concentrations,[44] however the potency of HNG in such small concentrations is unprecedented.

No significant denaturing of oligomeric IAPP was observed from HNG according to both molecular models and experiments (Figures 1, 2, and 6). HNG was also not significantly denatured in the presence of IAPP (Figure S2), however a number of transient secondary structures (helix-turn-bend) became more stabilized in crowded dimeric and trimeric environments. This suggests, perhaps, that the conformation of HNG may be more structured or stabilized in packed mitochondrial environments. Moreover, the stabilization of a short β-bend in the $_{11}$LLTGE$_{15}$ region of HNG appears to mediate the association with IAPP in β-stranded-to-disordered regions such as $_{25}$AILSS$_{29}$, as was observed in residue contact maps in Figure S6. This data also suggests that there may be reduced interactions between HNG and non-aggregating isoforms of IAPP such as rat IAPP, which contains multiple β-breaking prolines near this region.[45-46] As for other secondary structures, HNG did not appear to modulate the α-helical propensities of IAPP (not shown), which has been widely associated with its ability to permeabilize membranes.[37, 47-50]

Accessible free energy landscapes of HNG ensembles (Figure S1) reveal that although the radius of gyration remains at about 0.8-1.0 nm before and after binding to IAPP, the end-to-end distance of HNG is widely outspread at 3.0 nm in trimers compared to 0.5-3.0 nm in monomers and dimers. This is a result of HNG attempting to maximize contact with multiple NFGAIL regions on individual IAPP monomers, thus extending itself as far as possible. As observed in other IDPs,[29] the stabilized β-stranded structures adopted by IAPP dimers, trimers, and fibrils represent a subset of the states sampled by monomers in solution. Thus, IAPP aggregates do not inhabit fundamentally new states from IAPP monomers, but rather a stabilized subset of monomeric states that do not interconvert, consistent with the superposition of ensembles hypothesis.[29] Similarly, our use of protein end-to-end distances (R_{ee}) and radii of gyration (R_g) as IDP order parameters yield similar free energy landscapes to those plotted as functions of the protein RMSD,[51] suggesting that these observations are not artifacts of our particular order parameters.

The reduction of parallel IAPP hairpins in the presence of HNG (Figure 3) also mirrors our earlier observations with EPR.[14] In addition, those experiments revealed that HNG likely binds to IAPP oligomers,[14] rather than to monomers, which we have largely confirmed using molecular models. Figures 1 and 2 emphasize that monomeric IAPP is predominantly disordered, however HNG:IAPP heterodimers only occur in simulations when IAPP samples a β-stranded conformation, similar to its homodimeric and oligomeric state. It is unclear if soluble or pre-fibrillar IAPP adopts a distinct secondary structure from monomers or fibrils, although there is evidence that pre-fibrils remain disordered.[52] However, only a few energetically-unstable states exist where HNG interacts with disordered IAPP monomers, making disordered IAPP interactions unlikely. Instead, the most energetically-favorable states are between semi-β-stranded IAPP structures (referred to here as oligomeric) and HNG. This behavior is similar to other amyloid systems where membrane proteins and receptors only bind oligomeric amyloid complexes, but not disordered monomers.[53] Given that our umbrella sampling simulations (Figure 4) measured the adhesion between the most favorable heterodimer states, the large adhesion energy we report between HNG and IAPP (nearly 100 kT) represents the affinity between oligomeric IAPP and monomeric HNG, not the affinity between disordered IAPP and HNG. Subsequently, when HNG is bound to IAPP, additional IAPP bind to heterogeneous seeds with more affinity than to homogeneous IAPP seeds, however these interactions are still an order of magnitude weaker than between oligomeric IAPP and unscreened HNG monomers. While it cannot be ruled out from simulations that HNG stabilizes monomeric IAPP from a disordered-to-ordered state, it is much more likely that REMD captures the natural affinity between HNG and transiently-sampled IAPP hairpins.

The association between HNG and the NFGAIL region of IAPP is also reasonable given the well-established association between NFGAIL and IAPP aggregation.[20-23, 46] Additionally, interactions between HNG and the flanking regions directly following NFGAIL, which include a double serine repeat (Figure S6), are key observations from this study. Both of these serines are converted to prolines in non-aggregating rat IAPP,[46] and lie in the center of oligomeric IAPP β-strands in human IAPP. As a result, they represent an attractive hotspot for the docking-and-locking of incoming monomers, where HNG appears to cap and contain oligomers from recruiting additional IAPP. These flanking regions do not appear to affect the ability of IAPP to permeabilize membranes,[54] however they do help regulate, along with NFGAIL, the ability of IAPP to potently aggregate.[39] The strong attraction between HNG and IAPP-NFGAIL likely explains how mitochondrial peptides such as humanin are able to disrupt IAPP dimers so effectively, thereby reducing downstream aggregation. It is also interesting that the HNG isoform of humanin, despite being more cyto- and neuroprotective than its wildtype counterpart,[12-13] exhibits very few interactions between its unique S14G region and IAPP (Figure S3). This could suggest that the S14G mutation in HNG imparts greater conformational freedom for the monomer to bind to transient oligomeric β-sheets, rather than from direct interactions with the mutated residue. Currently, no systematic studies have differentiated the conformational heterogenity between wildtype humanin and HNG, however simulations comparing humanin isoforms are being actively pursued.

The adhesion of HNG to IAPP fibrils was also corroborated in MD using two independent structures from solid-state NMR[43] and from our earlier EPR experiments.[34] These structures capture disparate fibrillar morphologies that incorporate interactions between nearest neighbors and between more distant monomers. However, these fibrils and many others extracted through electron microscopy[34, 55] share an externalized NFGAIL fragment that is solvent-exposed, and which partially attracts HNG. This is due, in part, to the intrinsic disorder of the linker, which does not easily stabilize in experiments. Given that flanking regions around NFGAIL are partially buried in mature fibrils, they are likely indicators of an exposed and nucleation-prone IAPP interface for which HNG is most attracted to. Thus, the interactions observed here between HNG and IAPP fibrils, specifically near the NFGAILSS region of IAPP, is not expected to vary significantly with the inclusion of other fibril models or structures. It is the outward display of NFGAIL in oligomeric IAPP and the inner display of flanking amino acids that, taken together, facilitates a strong attraction to HNG which subsequently neutralizes the reactive interface.

Finally, joint ThT and electron microscopy experiments indicate that while HNG disrupts the primary and secondary nucleation of IAPP fibrils, it cannot deconstruct mature oligomers and fibrils. Consistent with our molecular models, HNG can only screen the nucleating interfaces of IAPP, whether they occur on the ends of fibrils or on the surface of NFGAIL-exposed surfaces. These results highlight the sub-stoichiometric potency of disordered peptides and peptide aptamers, especially in stabilizing environments such as the mitochondria where IDPs likely adopt more structured conformations. The unique ability of IDPs to carry out disparate functions in unique physiological environments suggests that they play a central role in the regulation of pathological protein structures, and may facilitate more targeted approaches to differentiate soluble amyloid oligomers from disordered monomers and classical amyloid fibrils.

CONCLUSIONS

In summary, this work highlights the fundamental biophysical interactions between the mitochondrial peptide HNG (humanin S14G) and IAPP, showing that miniscule amounts of mitochondrial IDPs can dramatically abrogate the formation of amyloid fibers. Molecular simulations corroborate both past and present experiments, further describing an amyloid inhibiting pathway that targets oligomeric IAPP through the aggregation-prone NFGAIL motif and its flanking amino acids. Conversely, this pathway does not lead to the dissolution of mature amyloid fibrils, though simulations indicate that HNG is capable of binding to mature IAPP fibrils. Binding of HNG to oligomeric IAPP, defined here as unbound or loosely-bound β-hairpins, caps and subsequently offsets additional IAPP from binding in optimal parallel β-sheet geometries, thereby destabilizing mature IAPP fibrils. These interactions are observed in heterodimers, trimers, and in fibrils, where HNG maximizes contact with NFGAIL and its flanking neighbors. HNG and IAPP do not significantly denature one another, however HNG becomes more structured in crowded protein environments compared to its disordered monomeric state. Thermodynamic ensembles reveal that HNG maximizes hydrophobic contact with IAPP through intermolecular hydrogen bonds with the IAPP backbone, though some intermolecular salt-bridges persist. Taken together, these results describe how endogenous IDPs can regulate pancreatic β-cell amyloids, which are a pathological hallmark of Type II Diabetes. These findings also highlight a number of amino acid targets in soluble amyloids that nucleate the formation of insoluble fibrils and plaques, thereby providing a biochemical target for mitigating the most cytotoxic amyloid species in Diabetes and in related amyloid diseases.

MATERIALS AND METHODS

Theoretical Modeling. Atomistic molecular dynamics simulations were carried out using the GROMACS 4.6.5 integrator.[56] The AMBER99sb-ILDN force fields [57] were utilized for modeling humanin S14G (seq. MAPRGFSCLLLLTGEIDLPVKRRA) and IAPP (seq. KCNTATCATQRLANFLVHSSNNFGAILSSTNVGSNTY), which were solvated with TIP3P water molecules.[58] The disulfide bond between the IAPP cysteine groups was maintained with a rigid constraint that could not be broken during the simulations, while the single histidine residue (with a hydrogen atom attached to the epsilon nitrogen) was neutralized. Newton's equations of motion were integrated over a 2 fs time step using a leapfrog algorithm. Short-range van der Waals and Coulomb potentials were truncated at 1.2 nm, while longer-ranged electrostatics were tabulated with Particle Mesh Ewald summation,[59] which reduces computation with Fast Fourier Transforms. Cartesian periodic boundary conditions were implemented in all directions to minimize the effects from unit-cell boundaries.

Protein Preparation in Simulations. Initial IAPP geometries were taken from previous studies,[60] where multiple energy-minimized IAPP conformations were identified under the AMBERFF96 force field[61] in an implicit solvent. These structures (which incorporated both α-helical and β-sheet conformations) were hydrated with an explicit solvent for 20 ns and seeded both the monomeric and dimeric replica-exchange ensembles. Humanin S14G (HNG) was constructed as a linear peptide chain using Avogadro 1.1.1,[62] and was allowed to partially fold for 20 ns before introduction as a replica-exchange seed. Since HNG and IAPP exhibited a net charge, chloride counter-ions were introduced to maintain charge neutrality. In each system, an NPT (constant number of atoms, pressure, and temperature) ensemble was maintained at 300 K and 1 bar of isotropic pressure using the weakly-coupled Berendsen barostat and thermostat,[63] which resulted in a box compressibility of 4.5E-5 bar^{-1} and box dimensions between 6-7 nm. Protein dimers and trimers were constructed by randomly pairing permutations of monomeric proteins and confirming that they remained dimerized or trimerized for at least 20 ns. For the protein trimer systems, two IAPP proteins were combined with a single HNG protein, however we did not attempt to combine two HNG proteins with a single IAPP protein due to limited computational resources.

Replica Exchange Molecular Dynamics. Replica-exchange molecular dynamics (REMD) ensembles[27] were constructed from IAPP and HNG seed systems that were converted to NVT (constant number of atoms, volume, and temperature) ensembles using the Nosé–Hoover thermostat,[64] which couples an external heat bath to the system Hamiltonian in order to construct a canonical thermodynamic ensemble. Protein chemical bonds were rigidly constrained with the linear constraint solver (LINCS),[65] while water bonds were constrained using the SETTLE algorithm,[66] which utilizes Lagrange multipliers to maintain holonomic constraints under a symplectic integrator. In order to increase the number of protein states sampled under REMD, replicas of the seed systems were duplicated and heated to temperatures ranging from 288 K to 500 K for monomers, and 288 K to 370 K for dimers and trimers. This yielded an ensemble containing 63 replicas for monomer simulations and 48 replicas for dimer and trimer simulations,

such that the Markovian exchange rate between replicas was fixed at 25% (with exchanges attempted every 3 ps). REMD simulations were run on average for 200 ns per replica, where the first 100 ns were ignored, and the second 100 ns were analyzed and summarized in this study. Combined, the replica-exchange component of this study represents over 64 μs of total atomistic computer simulation time, which was run using the XSEDE[67] platform on the Stampede2 supercomputer.

Computational Analysis. The GROMACS analysis tools g_hbond, g_traj, g_gyration, and g_cluster were employed to calculate the number of intra- and inter-molecular peptide bonds, protein end-to-end distances (R_{ee}), protein radii of gyration (R_g), and for protein clustering at room temperature. The high-temperature replicas were not analyzed in detail and were only used to populate the room temperature trajectory with energy-minimized protein structures. O-H hydrogen bonds were identified at distances at or below 2.5 Å, with an O-H-N angle at or below 30 degrees. The protein end-to-end distance – R_{ee} – was measured from the N-terminal center of mass to the C-terminal center of mass. Peptide clusters were tabulated using the Daura algorithm,[68] which groups protein backbones based on differences in their root mean square deviations ($d_{rms} \leq 2.0$ Å). Protein secondary structures were calculated using the DSSP tool.[69-70]

Potentials of Mean Force Simulations. Additional enhanced-sampling simulations were carried out on the most stable IAPP homodimers, IAPP-HNG heterodimers, and 2IAPP-1HNG trimers using Umbrella Sampling (US) simulations, all of which were re-normalized under the Weighted-Histogram Analysis Method – or WHAM.[28] Starting structures were chosen from the most dominant clusters in Figure 1. Each US simulation pulled an IAPP monomer away from a bound protein or protein cluster over a reaction coordinate spanning 3 nm, populated by 60 0.5 Å windows. The pull force on IAPP was maintained with a virtual spring ($k = 1000$ kJ/mol-nm^2) under an NVT ensemble and was used to sample the potential of mean force over 25 ns per bin. Overall, this represents an additional 4.5 μs of simulation time to ascertain the binding free energy of IAPP to multiple structures.

Fibril Simulations. IAPP fibril structures were adapted from both our previous EPR studies[34] and from solid-state NMR by Tycko et al.[43] Fibrils were combined with a single HNG monomer placed in bulk solution, and standard molecular dynamics simulations were run for 100 ns at room temperature to evaluate potential HNG-IAPP binding sites. Protein force fields and thermodynamic variables were identical to the REMD simulations, and analyses were conducted only on the second half (50 ns) of the simulation.

Materials and Chemicals. Wild-type human IAPP was purchased from Bachem America (Torrance, CA). Humanin S14G (HNG) was purchased from Genscript (Piscataway, NJ). 8M guanidinium chloride and thioflavin T were obtained from Sigma-Aldrich (Milwaukee, WI).

Peptide Handling and Storage. IAPP was dissolved in HFIP, aliquoted into tubes, flash frozen and then lyophilized overnight. IAPP concentration was determined by UV absorbance at 280 nm in

8M guanidinium chloride using an extinction coefficient of 1405 $M^{-1}cm^{-1}$. Lyophilized IAPP stocks were sealed in $N_2(g)$ and stored under vacuum until use. HNG was solubilized in water at 1 mg/ml, aliquoted into tubes, and then stored in -80 °C until use.

Thioflavin T Fluorescence Assay. Lyophilized IAPP was solubilized at 100 μM with 5% seed in 10 mM potassium phosphate buffer (pH 7.4) and allowed to fibrilize for at least 48 hours at room temperature without agitation.

For the fibril stability tests, HNG or guanidium were added to appropriate reactions so that the final IAPP and ThT concentrations were 12.5 μM and the fluorescence was measured for 24 hours. The IAPP samples in each condition were taken from an identical batch of fibrils. Student t-test was performed to compare ThT fluorescence endpoints.

ThT fluorescence was measured using an Eppendorf AF2200 plate reader. Samples were loaded into falcon 96-well plates with a sample volume of 60 μL. The excitation wavelength was 440 nm (bandwidth of 30 nm), while the emission wavelength was 480 nm (40 nm bandwidth).

Transmission Electron Microscopy. Samples were applied to formvar carbon film on copper mesh grids for at least 10 minutes. The excess liquid was blotted away and then the sample was negatively stained with 1% uranyl acetate for 3 minutes. Grids were imaged on a JEOL-1400 Transmission Electron Microscope operated at 100 kV.

ACKOWLEDGEMENTS

J.E.S. acknowledges support from the NSF (MCB-1716956). This work used the Extreme Science and Engineering Discovery Environment (XSEDE), which is supported by National Science Foundation grant number ACI-1548562. Computation on XSEDE was made possible through the allocations TG-MCA05S027 and TG-MCB170142. The authors also acknowledge the Texas Advanced Computing Center (TACC) at the University of Texas at Austin for providing high performance computing resources that have contributed to the research results reported within this paper. Partial financial support was provided by the California Nanosystems Institute (CNSI) under NSF grant CNS-1725797 and the NSF MRSEC at UCSB under the NSF grant DMR-1720256.

FIGURES

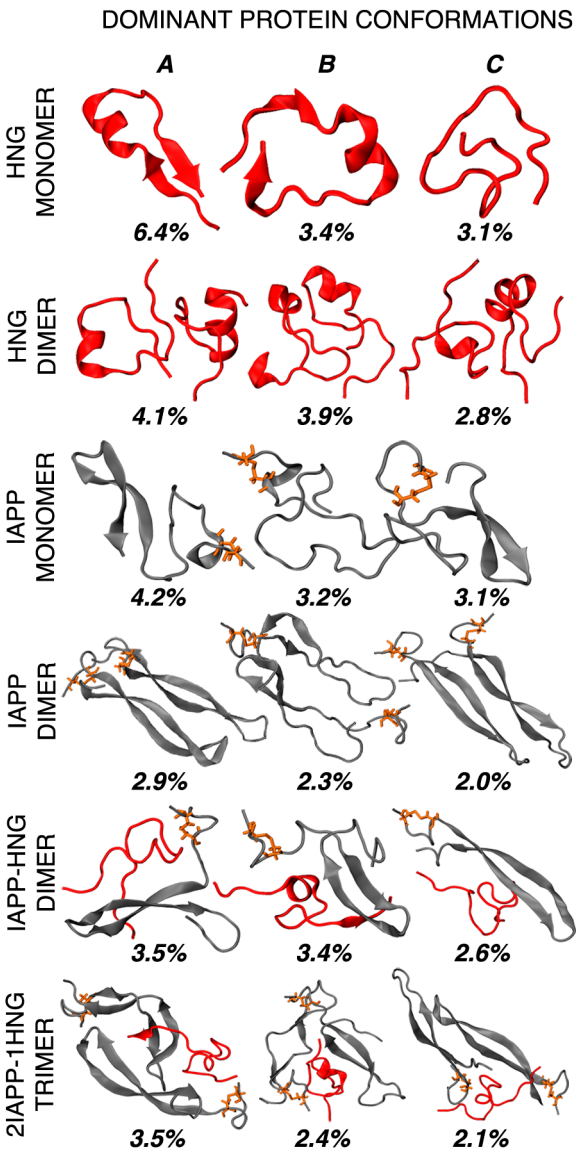

Figure 1. The most dominant protein clusters [A-C] for HNG (red) and IAPP (gray) mixtures reveal that the proteins do not denature one another, but instead offset aggregation-prone geometries. Residency times in each cluster are displayed below each representative snapshot, while the IAPP disulfide bridge is explicitly shown in orange.

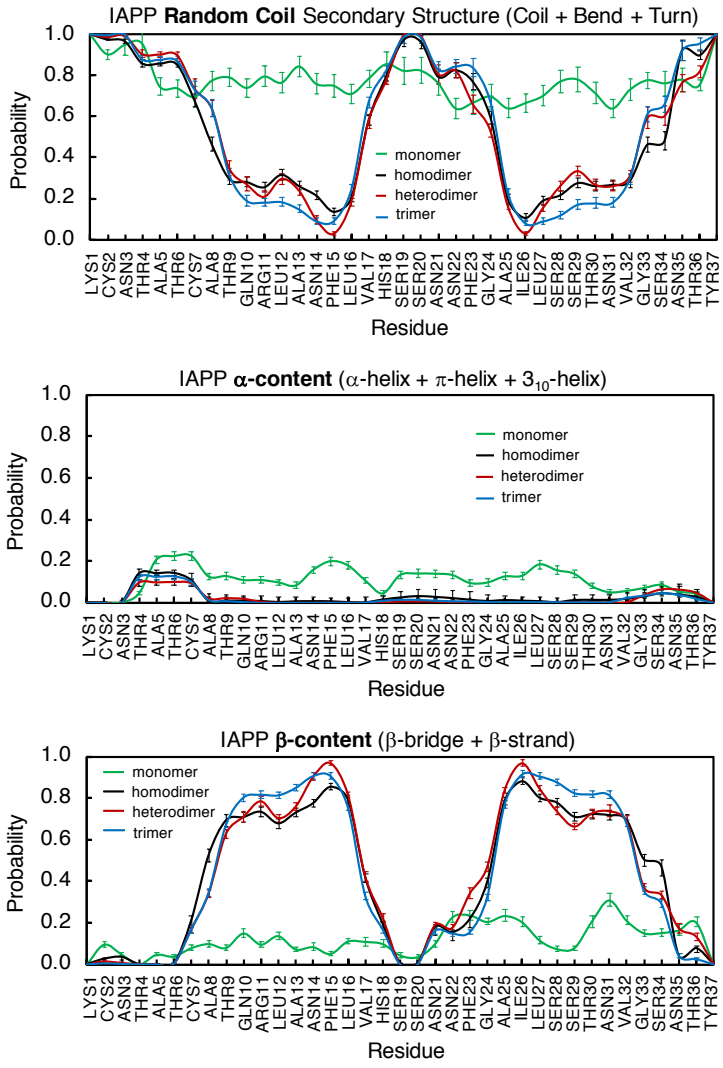

Figure 2. Average IAPP secondary structures reveal a similar disordered-to-ordered transition upon binding to either IAPP or HNG. Only the disordered linker at the center of IAPP remains disordered, while the surrounding regions (including $_{22}$NFGAIL$_{27}$) gain significant β-content. Heterodimers exhibit similar secondary structures to homodimers, though there is a marginal increase in IAPP β-propensity when HNG is present.

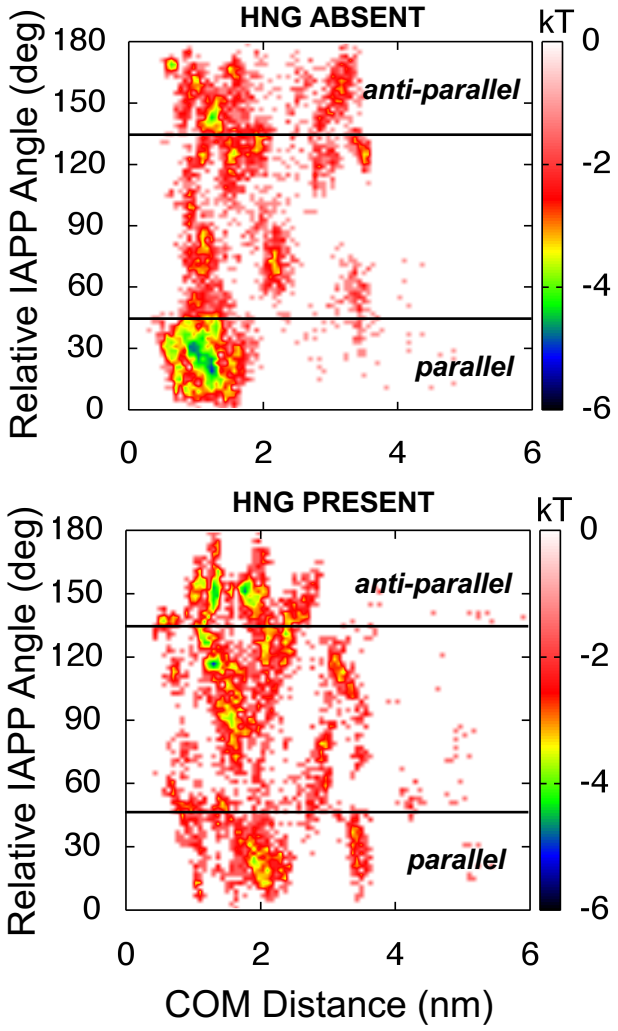

Figure 3. Relative IAPP orientation is potently affected by HNG monomers, as revealed by free energy landscapes (FELs). Low-energy basins (in blue and green) reveal that IAPP homodimers prefer to populate closely-packed parallel conformations, however the introduction of HNG inhibits or separates most parallel assemblies in favor of anti-parallel IAPP orientations.

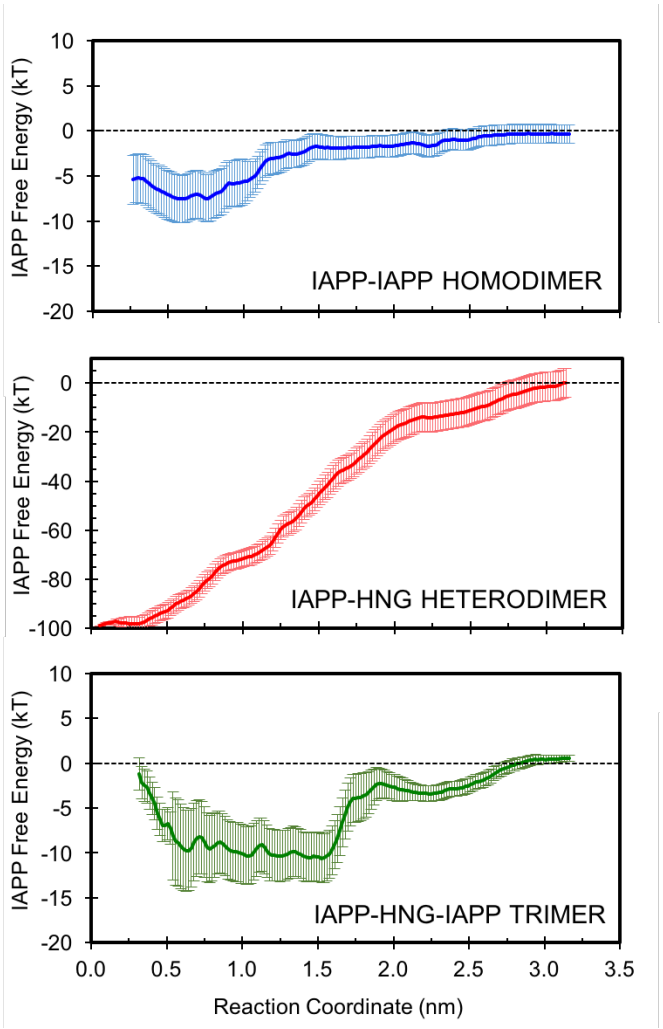

Figure 4 Potentials of mean force on IAPP when separated from an IAPP monomer (homodimer), an HNG monomer (heterodimer), and an IAPP-HNG dimer (trimer). Umbrella sampling simulations reveal that IAPP is ten times more adhesive to β-stabilized HNG compared to other IAPP. Similarly, IAPP adhesion in mixed trimers is greater than in homogeneous dimers due to the presence of the embedded HNG protein.

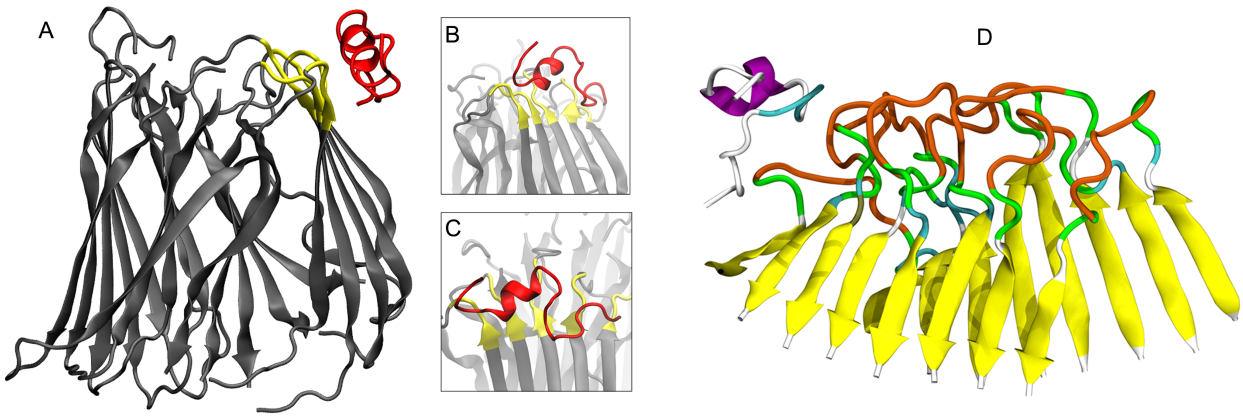

Figure 5. *Left:* IAPP fibrils from NMR[43] (gray) bind HNG (red) to flanking regions near the aggregation-prone NFGAIL region (yellow). Multiple simulation snapshots [A-C] suggest that HNG splays across multiple NFGAIL motifs, likely capping subsequent fibril growth. *Right*: HNG also binds to IAPP fibrils from EPR[34] near NFGAIL (orange) and its SS and SN flanking regions (green), located towards the binding interface on the fibril edge.

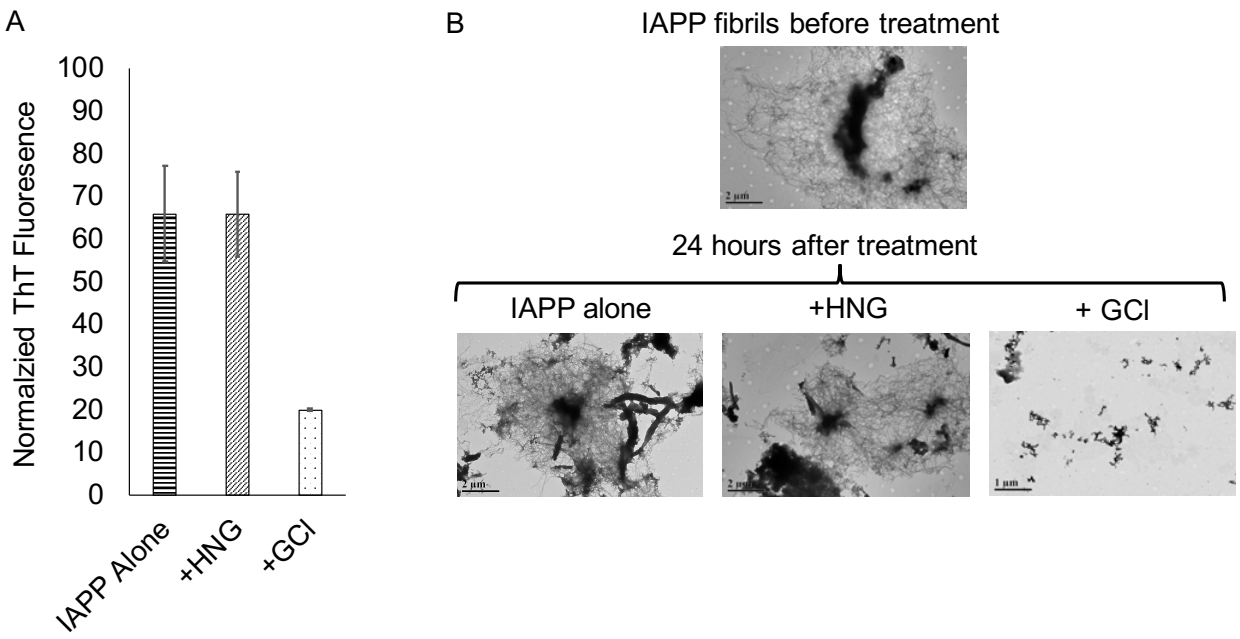

Figure 6. [A] HNG does not alter ThT fluorescence of pre-formed IAPP fibrils. ThT fluorescence of 12.5 μM of pre-formed IAPP fibrils alone (horizontal lines) or in the presence of 12.5 μM HNG (diagonal lines) or 4 M guanidinium chloride (dotted lines). While the addition of guanidinium causes a pronounced reduction in ThT fluorescence, the addition of HNG did not cause any noticeable ThT fluorescence changes. Fluorescence values were normalized to the starting value of IAPP fibrils alone. Error bar represent the standard deviation across 3 wells for IAPP alone and +HNG, and across 2 wells for +GCl (P-value $\leqq$ 0.015). [B] HNG does not dissolve IAPP fibrils according to electron microscopy. Images of negatively stained samples were obtained for untreated IAPP as well as samples treated with 12.5 μM HNG or 4 M guanidinium chloride.

SUPPLEMENTARY FIGURES

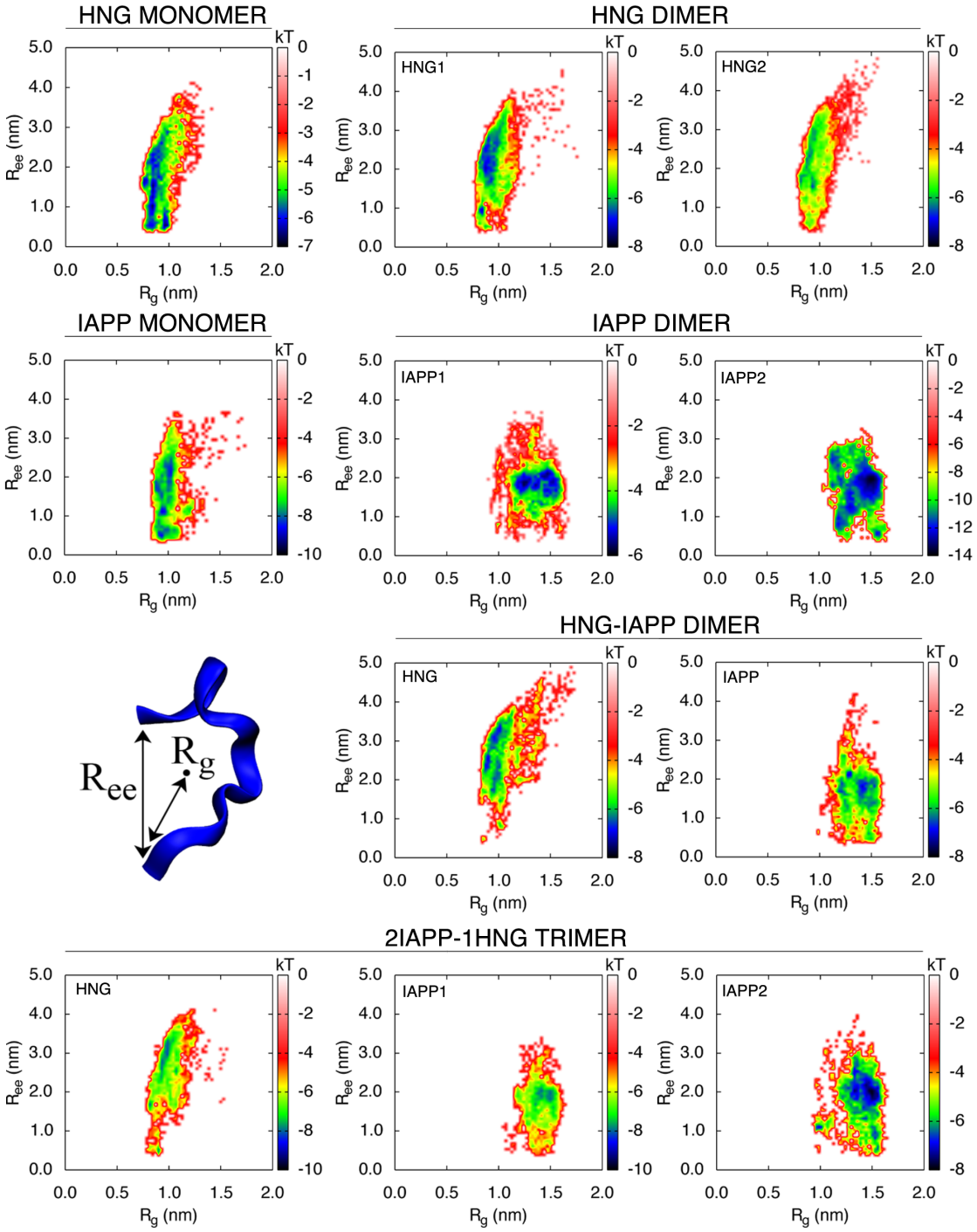

Figure S1. Free energy landscapes (FELs) from REMD reveal low-lying conformational basins that stabilize energy-minimized protein states (in blue) as a function of the protein end-to-end distance (R_{ee}) and radius of gyration (R_g). Mixing of HNG and IAPP proteins do not substantially modify the conformational ensembles that each protein inhabits.

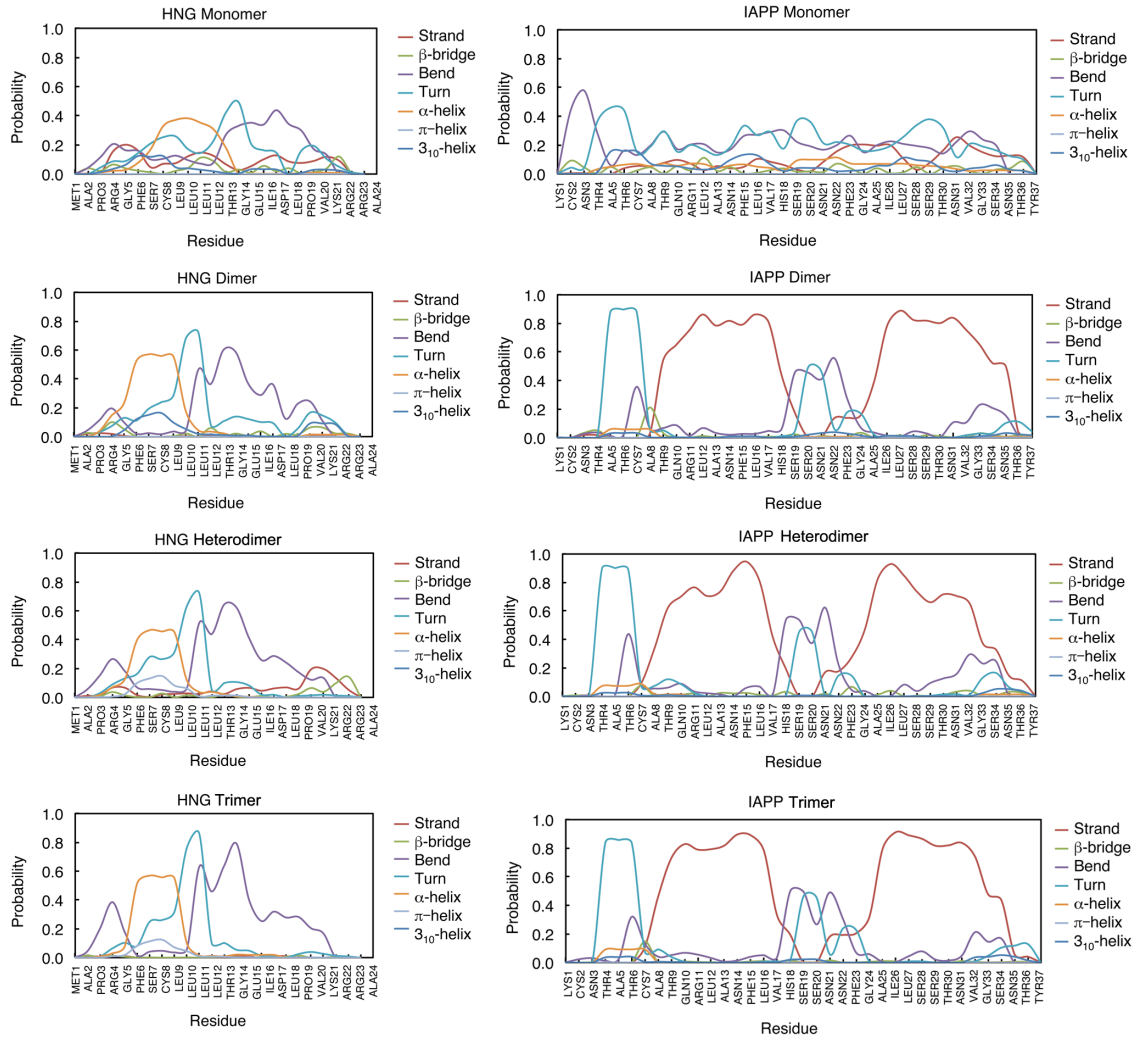

Figure S2. Dominant secondary structures for HNG (left) and IAPP (right) in monomeric (top row), homodimeric (second row), heterodimeric (third row), and trimeric (bottom row) states. IAPP β-strands are immediately stabilized in the presence of neighbors, however HNG secondary structures are only moderately stabilized when the protein is bound to neighbors.

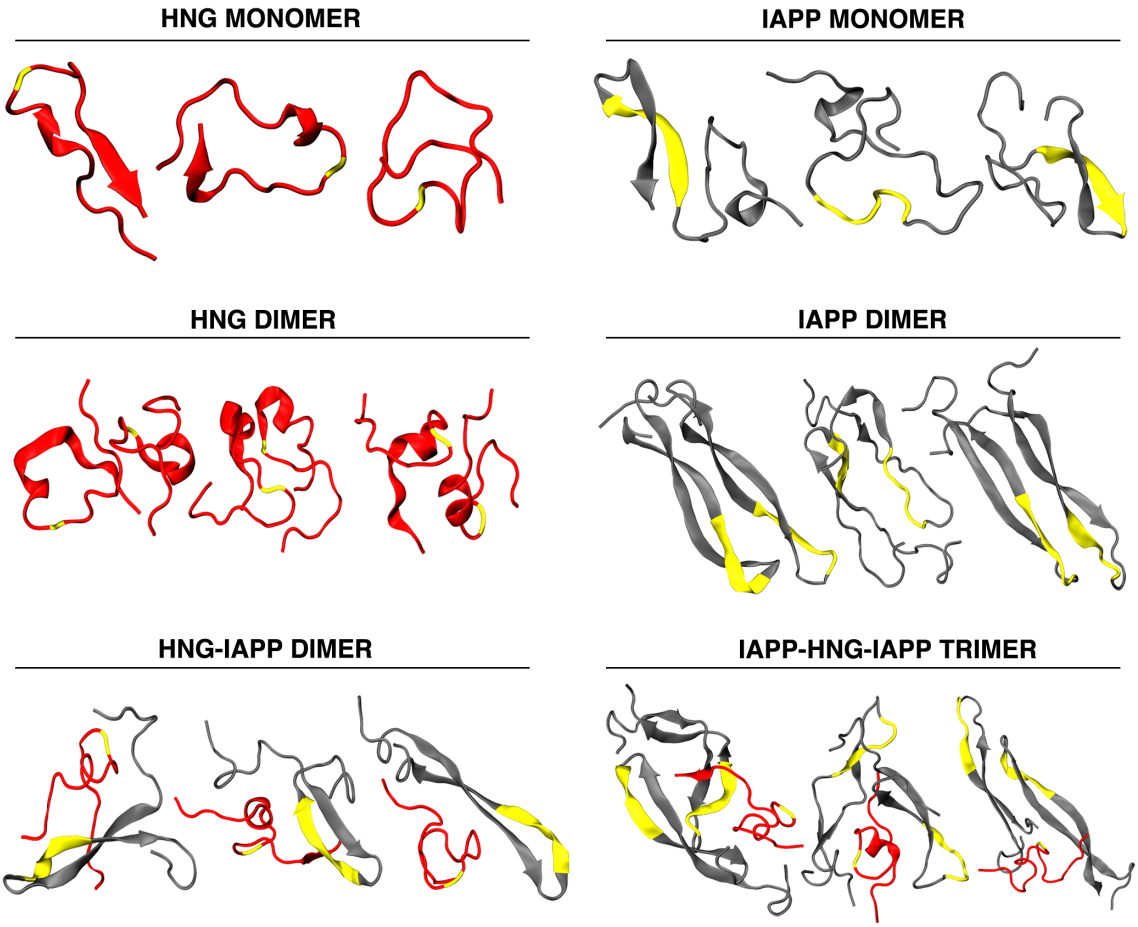

Figure S3. The HNG Gly14 residue and the IAPP-NFGAIL group (highlighted in yellow) are shown in the most dominant protein conformations. Gly14 (mutated from Ser14) does not appear to significantly affect the resulting HNG (red) morphologies. However, the IAPP (gray) NFGAIL region, which has been associated with pathological IAPP aggregation, is usually paired during IAPP dimerization, but is separated upon insertion of HNG.

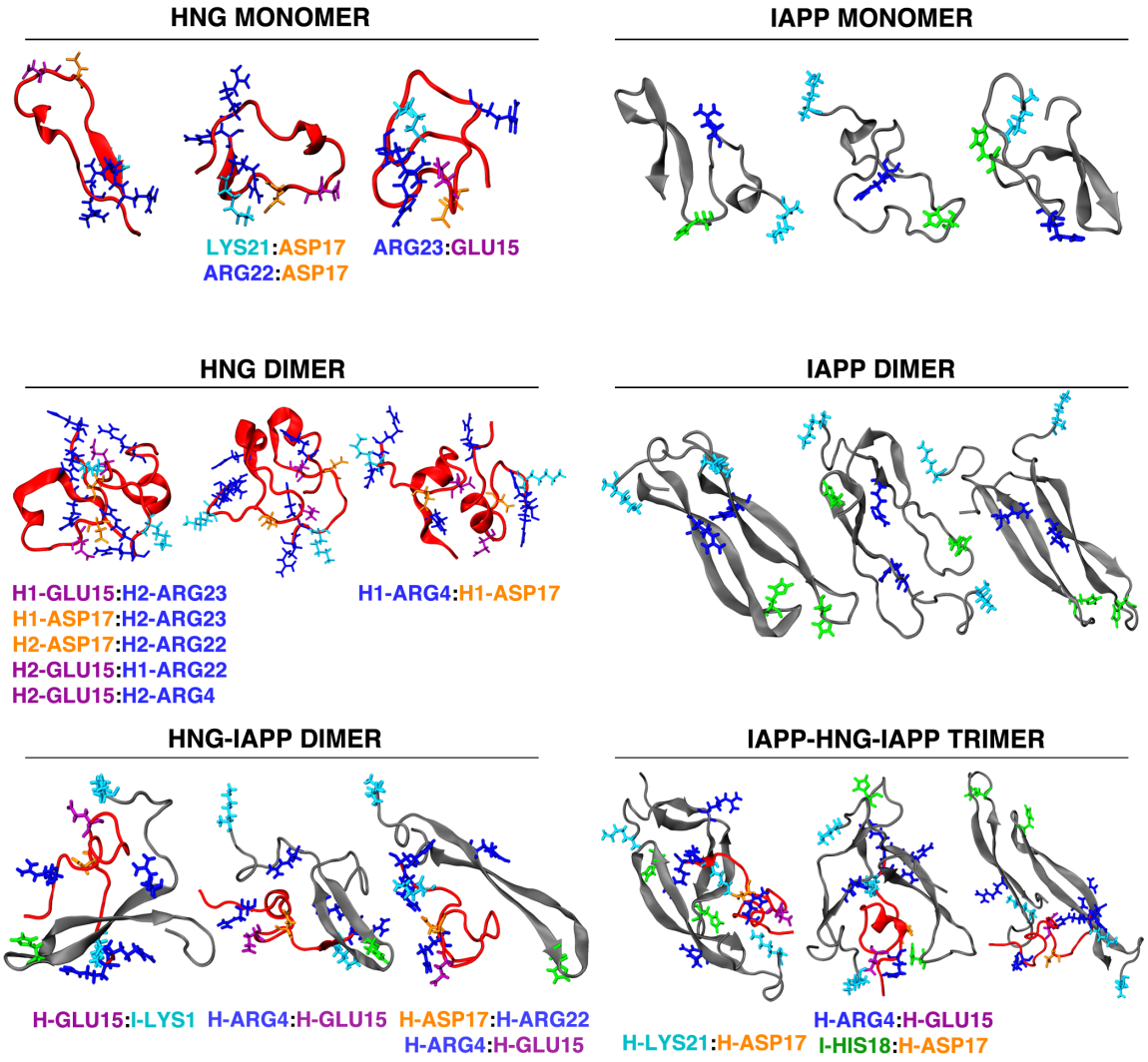

Figure S4. Salt bridges and electrostatic interactions between charged amino acids are highlighted for each of the dominant HNG (red) and IAPP (gray) protein clusters. While a large number of intra- and inter-molecular salt bridges exist in HNG dimers, heterodimers and trimers are not significantly stabilized by electrostatic interactions, but rather through hydrogen-bonding.

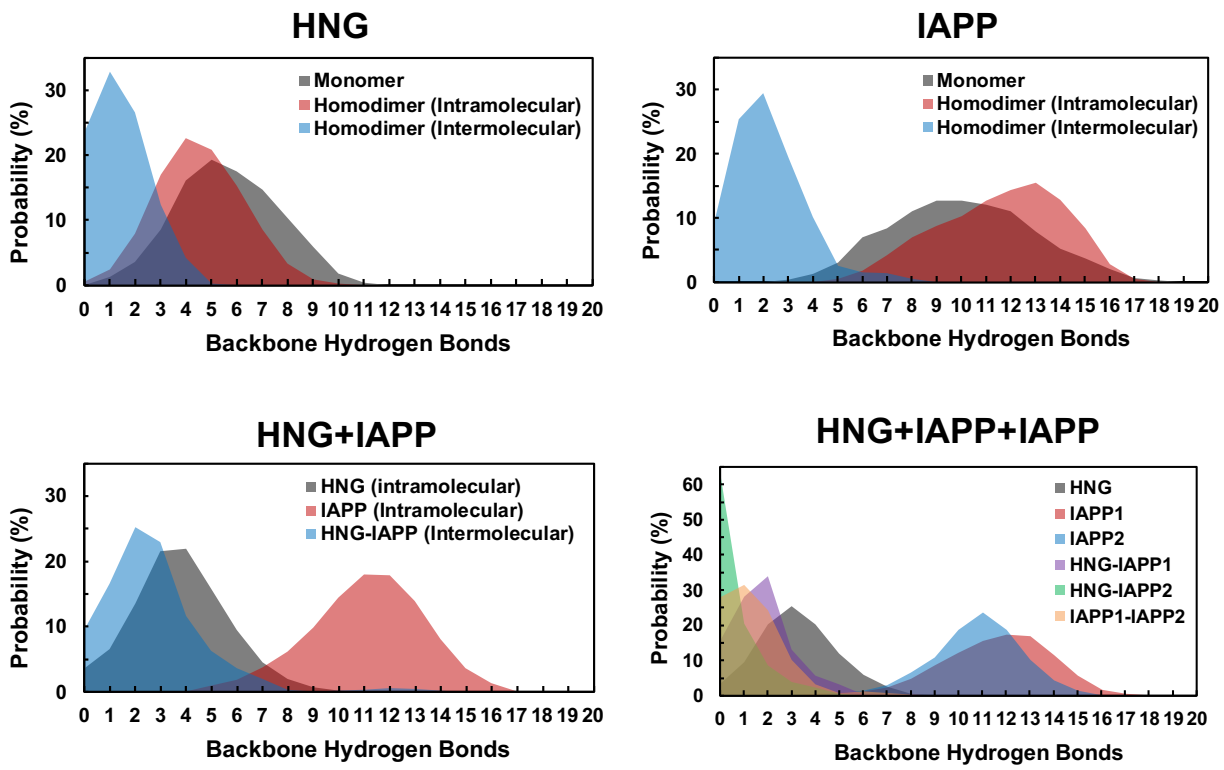

Figure S5. REMD simulations reveal the distributions of intra- and inter-molecular hydrogen bonds formed between protein backbones. IAPP monomers tend to exhibit more backbone hydrogen bonds per residue (0.25) compared to HNG monomers (0.20). Upon dimerization, HNG homodimers convert one backbone intramolecular hydrogen bond to an intermolecular backbone hydrogen bond while IAPP homodimers gain two intermolecular and four intramolecular hydrogen bonds. These trends are also observed in heterogeneous oligomers.

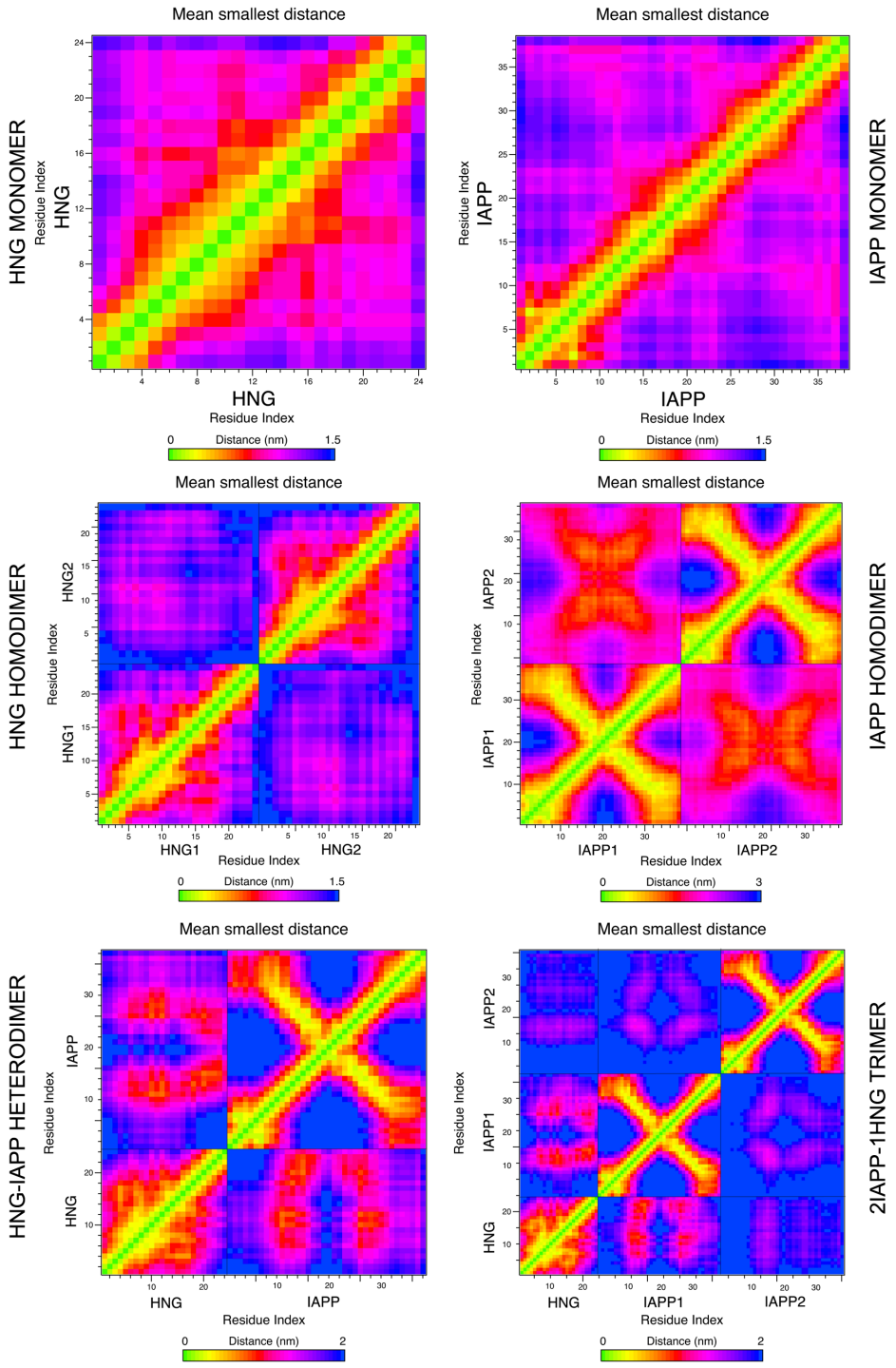

Figure S6. Protein contact maps from REMD simulations. Monomers exhibit very little intramolecular association, however intermolecular contact maps show close contact between $_{12}$LANFLV$_{17}$ and $_{22}$NFGAIL$_{27}$ regions in IAPP, representing a combination of parallel and anti-parallel strands. Heterodimer contact maps reveal an association between HNG-$_{9}$LLLL$_{12}$ and IAPP-$_{11}$RLA$_{13}$ or IAPP-$_{26}$ILS$_{28}$, and HNG-$_{20}$VKR$_{22}$ and IAPP-$_{13}$ANF$_{15}$ or IAPP-$_{25}$AIL$_{27}$.

REFERENCES

1. Andersson, G.; Karlberg, O.; Canbäck, B.; Kurland, C. G., On the origin of mitochondria: a genomics perspective. *Philosophical Transactions of the Royal Society of London B: Biological Sciences* **2003,** *358* (1429), 165-179.
2. Hollenberg, C.; Borst, P.; Van Bruggen, E., Mitochondrial DNA: V. A 25-μ closed circular duplex DNA molecule in wild-type yeast mitochondria. Structure and genetic complexity. *Biochimica et Biophysica Acta (BBA)-Nucleic Acids and Protein Synthesis* **1970,** *209* (1), 1-15.
3. Taanman, J.-W., The mitochondrial genome: structure, transcription, translation and replication. *Biochimica et Biophysica Acta (BBA)-Bioenergetics* **1999,** *1410* (2), 103-123.
4. Attardi, G.; Schatz, G., Biogenesis of mitochondria. *Annual review of cell biology* **1988,** *4* (1), 289-331.
5. Anderson, S.; Bankier, A. T.; Barrell, B. G.; De Bruijn, M.; Coulson, A. R.; Drouin, J.; Eperon, I.; Nierlich, D.; Roe, B. A.; Sanger, F., Sequence and organization of the human mitochondrial genome. **1981**.
6. Hashimoto, Y.; Niikura, T.; Tajima, H.; Yasukawa, T.; Sudo, H.; Ito, Y.; Kita, Y.; Kawasumi, M.; Kouyama, K.; Doyu, M., A rescue factor abolishing neuronal cell death by a wide spectrum of familial Alzheimer's disease genes and Aβ. *Proceedings of the National Academy of Sciences* **2001,** *98* (11), 6336-6341.
7. Guo, B.; Zhai, D.; Cabezas, E.; Welsh, K.; Nouraini, S.; Satterthwait, A. C.; Reed, J. C., Humanin peptide suppresses apoptosis by interfering with Bax activation. *Nature* **2003,** *423* (6938), 456-461.
8. Ikonen, M.; Liu, B.; Hashimoto, Y.; Ma, L.; Lee, K.-W.; Niikura, T.; Nishimoto, I.; Cohen, P., Interaction between the Alzheimer's survival peptide humanin and insulin-like growth factor-binding protein 3 regulates cell survival and apoptosis. *Proceedings of the National Academy of Sciences* **2003,** *100* (22), 13042-13047.
9. Krejcova, G.; Patocka, J.; Slaninova, J., Effect of humanin analogues on experimentally induced impairment of spatial memory in rats. *Journal of Peptide Science* **2004,** *10* (10), 636-639.
10. Mamiya, T.; Ukai, M., [Gly14]-Humanin improved the learning and memory impairment induced by scopolamine in vivo. *Brit J Pharmacol* **2001,** *134* (8), 1597-1599.
11. Widmer, R. J.; Flammer, A.; Herrmann, J.; Rodriguez-Porcel, M.; Wan, J.; Cohen, P.; Lerman, L. O.; Lerman, A., Circulating humanin levels are associated with preserved coronary endothelial function. *American Journal of Physiology-Heart and Circulatory Physiology* **2013,** *304* (3), H393-H397.
12. Tajima, H.; Kawasumi, M.; Chiba, T.; Yamada, M.; Yamashita, K.; Nawa, M.; Kita, Y.; Kouyama, K.; Aiso, S.; Matsuoka, M., A humanin derivative, S14G-HN, prevents amyloid-β-induced memory impairment in mice. *Journal of neuroscience research* **2005,** *79* (5), 714-723.
13. Zhang, W.; Zhang, W.; Li, Z.; Hao, J.; Zhang, Z.; Liu, L.; Mao, N.; Miao, J.; Zhang, L., S14G-humanin improves cognitive deficits and reduces amyloid pathology in the middle-aged APPswe/PS1dE9 mice. *Pharmacology Biochemistry and Behavior* **2012,** *100* (3), 361-369.
14. Okada, A. K.; Teranishi, K.; Lobo, F.; Isas, J. M.; Xiao, J.; Yen, K.; Cohen, P.; Langen, R., The Mitochondrial-Derived Peptides, HumaninS14G and Small Humanin-like Peptide 2, Exhibit Chaperone-like Activity. *Sci Rep-Uk* **2017,** *7* (1), 7802.
15. Junghans, A.; Watkins, E. B.; Majewski, J.; Miranker, A.; Stroe, I., Influence of the Human and Rat Islet Amyloid Polypeptides on Structure of Phospholipid Bilayers: Neutron Reflectometry and Fluorescence Microscopy Studies. *Langmuir* **2016,** *32* (17), 4382-4391.

16. Birol, M.; Kumar, S.; Rhoades, E.; Miranker, A. D., Conformational switching within dynamic oligomers underpins toxic gain-of-function by diabetes-associated amyloid. *Nature communications* **2018,** *9* (1), 1312.
17. Birol, M.; Kumar, S.; Rhoades, E.; Miranker, A. D., Structurally distinct oligomers of islet amyloid polypeptide mediate toxic and non-toxic membrane poration. *bioRxiv* **2016**, 095158.
18. Wojcik, S.; Birol, M.; Rhoades, E.; Miranker, A. D.; Levine, Z. A., Targeting the Intrinsically Disordered Proteome Using Small-Molecule Ligands. *Methods Enzymol* **2018,** *611*, 703-734.
19. Organization, W. H., Diabetes Fact sheet N 312. 2012. *World Health Organization* **2010**.
20. Zanuy, D.; Ma, B.; Nussinov, R., Short peptide amyloid organization: stabilities and conformations of the islet amyloid peptide NFGAIL. *Biophysical journal* **2003,** *84* (3), 1884-1894.
21. Wu, C.; Lei, H.; Duan, Y., Elongation of Ordered Peptide Aggregate of an Amyloidogenic Hexapeptide NFGAIL Observed in Molecular Dynamics Simulations with Explicit Solvent. *Journal of the American Chemical Society* **2005,** *127* (39), 13530-13537.
22. Sellin, D.; Yan, L. M.; Kapurniotu, A.; Winter, R., Suppression of IAPP fibrillation at anionic lipid membranes via IAPP-derived amyloid inhibitors and insulin. *Biophysical Chemistry* **2010,** *150* (1-3), 73-79.
23. Cai, Z. W.; Li, J. Q.; Yin, C. J.; Yang, Z. X.; Wu, J. L.; Zhou, R. H., Effect of Urea Concentration on Aggregation of Amyloidogenic Hexapeptides (NFGAIL). *Journal of Physical Chemistry B* **2014,** *118* (1), 48-57.
24. Abedini, A.; Meng, F. L.; Raleigh, D. P., A single-point mutation converts the highly amyloidogenic human islet amyloid polypeptide into a potent fibrillization inhibitor. *Journal of the American Chemical Society* **2007,** *129* (37), 11300-+.
25. Sivanesam, K.; Andersen, N. H., Inhibition of Human Amylin Amyloidogenesis by Human Amylin-Fragment Peptides: Exploring the Effects of Serine Residues and Oligomerization upon Inhibitory Potency. *Biochemistry* **2017,** *56* (40), 5373-5379.
26. Darrow, M. C.; Sergeeva, O. A.; Isas, J. M.; Galaz-Montoya, J. G.; King, J. A.; Langen, R.; Schmid, M. F.; Chiu, W., Structural Mechanisms of Mutant Huntingtin Aggregation Suppression by the Synthetic Chaperonin-like CCT5 Complex Explained by Cryoelectron Tomography. *Journal of Biological Chemistry* **2015,** *290* (28), 17451-17461.
27. Sugita, Y.; Okamoto, Y., Replica-exchange molecular dynamics method for protein folding. *Chemical Physics Letters* **1999,** *314* (1-2), 141-151.
28. Souaille, M.; Roux, B. t., Extension to the weighted histogram analysis method: combining umbrella sampling with free energy calculations. *Comput Phys Commun* **2001,** *135* (1), 40-57.
29. Levine, Z. A.; Larini, L.; LaPointe, N. E.; Feinstein, S. C.; Shea, J.-E., Regulation and aggregation of intrinsically disordered peptides. *Proceedings of the National Academy of Sciences* **2015,** *112* (9), 2758-2763.
30. Sawaya, M. R.; Sambashivan, S.; Nelson, R.; Ivanova, M. I.; Sievers, S. A.; Apostol, M. I.; Thompson, M. J.; Balbirnie, M.; Wiltzius, J. J.; McFarlane, H. T.; Madsen, A. O.; Riekel, C.; Eisenberg, D., Atomic structures of amyloid cross-beta spines reveal varied steric zippers. *Nature* **2007,** *447* (7143), 453-7.
31. Dupuis, N. F.; Wu, C.; Shea, J. E.; Bowers, M. T., Human Islet Amyloid Polypeptide Monomers Form Ordered beta-hairpins: A Possible Direct Amyloidogenic Precursor. *Journal of the American Chemical Society* **2009,** *131* (51), 18283-18292.
32. Laghaei, R.; Mousseau, N.; Wei, G. H., Effect of the Disulfide Bond on the Monomeric Structure of Human Amylin Studied by Combined Hamiltonian and Temperature Replica

Exchange Molecular Dynamics Simulations. *Journal of Physical Chemistry B* **2010,** *114* (20), 7071-7077.
33. Laghaei, R.; Mousseau, N.; Wei, G. H., Structure and Thermodynamics of Amylin Dimer Studied by Hamiltonian-Temperature Replica Exchange Molecular Dynamics Simulations. *Journal of Physical Chemistry B* **2011,** *115* (12), 3146-3154.
34. Bedrood, S.; Li, Y.; Isas, J. M.; Hegde, B. G.; Baxa, U.; Haworth, I. S.; Langen, R., Fibril Structure of Human Islet Amyloid Polypeptide. *Journal of Biological Chemistry* **2012,** *287* (8), 5235-5241.
35. Levine, Z. A.; Shea, J.-E., Simulations of disordered proteins and systems with conformational heterogeneity. *Current opinion in structural biology* **2017,** *43*, 95-103.
36. Levine, Z. A.; Rapp, M. V.; Wei, W.; Mullen, R. G.; Wu, C.; Zerze, G. H.; Mittal, J.; Waite, J. H.; Israelachvili, J. N.; Shea, J.-E., Surface force measurements and simulations of mussel-derived peptide adhesives on wet organic surfaces. *Proceedings of the National Academy of Sciences* **2016**.
37. Schlamadinger, D. E.; Kumar, S.; Magzoub, M.; Hebda, J. A.; Miranker, A. D., Inhibition and Mechanism of Islet Amyloid Polypeptide Toxicity. *Biophysical Journal* **2013,** *104* (2), 56a-56a.
38. Ruschak, A. M.; Miranker, A. D., Fiber-dependent amyloid formation as catalysis of an existing reaction pathway. *Proc Natl Acad Sci U S A* **2007,** *104* (30), 12341-6.
39. Ruschak, A. M.; Miranker, A. D., The role of prefibrillar structures in the assembly of a peptide amyloid. *J Mol Biol* **2009,** *393* (1), 214-26.
40. Benaki, D.; Zikos, C.; Evangelou, A.; Livaniou, E.; Vlassi, M.; Mikros, E.; Pelecanou, M., Solution structure of humanin, a peptide against Alzheimer's disease-related neurotoxicity. *Biochemical and Biophysical Research Communications* **2005,** *329* (1), 152-160.
41. Yan, L.-M.; Tatarek-Nossol, M.; Velkova, A.; Kazantzis, A.; Kapurniotu, A., Design of a mimic of nonamyloidogenic and bioactive human islet amyloid polypeptide (IAPP) as nanomolar affinity inhibitor of IAPP cytotoxic fibrillogenesis. *Proceedings of the National Academy of Sciences of the United States of America* **2006,** *103* (7), 2046-2051.
42. Torrie, G. M.; Valleau, J. P., Nonphysical sampling distributions in Monte Carlo free-energy estimation: Umbrella sampling. *J Comput Phys* **1977,** *23* (2), 187-199.
43. Luca, S.; Yau, W.-M.; Leapman, R.; Tycko, R., Peptide conformation and supramolecular organization in amylin fibrils: Constraints from solid state NMR. *Biochemistry* **2007,** *46* (47), 13505.
44. Wiltzius, J. J. W.; Sievers, S. A.; Sawaya, M. R.; Eisenberg, D., Atomic structures of IAPP (amylin) fusions suggest a mechanism for fibrillation and the role of insulin in the process. *Protein Sci* **2009,** *18* (7), 1521-1530.
45. Wu, C.; Shea, J. E., Structural Similarities and Differences between Amyloidogenic and Non-Amyloidogenic Islet Amyloid Polypeptide (IAPP) Sequences and Implications for the Dual Physiological and Pathological Activities of These Peptides. *Plos Comput Biol* **2013,** *9* (8).
46. Chiu, C.-c.; Singh, S.; de Pablo, Juan J., Effect of Proline Mutations on the Monomer Conformations of Amylin. *Biophysical Journal* **2013,** *105* (5), 1227-1235.
47. Kumar, S.; Schlamadinger, D. E.; Brown, M. A.; Dunn, J. M.; Mercado, B.; Hebda, J. A.; Saraogi, I.; Rhoades, E.; Hamilton, A. D.; Miranker, A. D., Islet Amyloid-Induced Cell Death and Bilayer Integrity Loss Share a Molecular Origin Targetable with Oligopyridylamide-Based alpha-Helical Mimetics. *Chem Biol* **2015,** *22* (3), 369-378.

48. Kumar, S.; Schlamadinger, D. E.; Miranker, A., Targeting Protein Misfolding(Islet Amyloid Polypeptide) using Helical Mimetics. *Biophysical Journal* **2013,** *104* (2), 379a-379a.
49. Last, N. B.; Rhoades, E.; Miranker, A. D., Islet amyloid polypeptide demonstrates a persistent capacity to disrupt membrane integrity. *Proceedings of the National Academy of Sciences* **2011,** *108* (23), 9460-9465.
50. Apostolidou, M.; Jayasinghe, S. A.; Langen, R., Structure of alpha-helical membrane-bound human islet amyloid polypeptide and its implications for membrane-mediated misfolding. *J Biol Chem* **2008,** *283* (25), 17205-10.
51. Levine, Z. A.; Fischer, S. A.; Shea, J.-E.; Pfaendtner, J., Trp-Cage Folding on Organic Surfaces. *The Journal of Physical Chemistry B* **2015,** *119* (33), 10417-10425.
52. Mishra, R.; Geyer, M.; Winter, R., NMR Spectroscopic Investigation of Early Events in IAPP Amyloid Fibril Formation. *Chembiochem* **2009,** *10* (11), 1769-1772.
53. Lauren, J.; Gimbel, D. A.; Nygaard, H. B.; Gilbert, J. W.; Strittmatter, S. M., Cellular prion protein mediates impairment of synaptic plasticity by amyloid-beta oligomers. *Nature* **2009,** *457* (7233), 1128-32.
54. Nanga, R. P. R.; Brender, J. R.; Xu, J.; Veglia, G.; Ramamoorthy, A., Structures of rat and human islet amyloid polypeptide IAPP1–19 in micelles by NMR spectroscopy. *Biochemistry* **2008,** *47* (48), 12689.
55. Li, Y.; Hatmal, M. m. M.; Langen, R.; Haworth, I. S., Idealized Models of Protofilaments of Human Islet Amyloid Polypeptide. *J Chem Inf Model* **2012,** *52* (11), 2983-2991.
56. Hess, B.; Kutzner, C.; van der Spoel, D.; Lindahl, E., GROMACS 4: Algorithms for highly efficient, load-balanced, and scalable molecular simulation. *Journal of Chemical Theory and Computation* **2008,** *4* (3), 435-447.
57. Lindorff-Larsen, K.; Piana, S.; Palmo, K.; Maragakis, P.; Klepeis, J. L.; Dror, R. O.; Shaw, D. E., Improved side-chain torsion potentials for the Amber ff99SB protein force field. *Proteins: Structure, Function, and Bioinformatics* **2010,** *78* (8), 1950-1958.
58. Jorgensen, W. L.; Chandrasekhar, J.; Madura, J. D.; Impey, R. W.; Klein, M. L., Comparison of Simple Potential Functions for Simulating Liquid Water. *Journal of Chemical Physics* **1983,** *79* (2), 926-935.
59. Essmann, U.; Perera, L.; Berkowitz, M. L.; Darden, T.; Lee, H.; Pedersen, L. G., A Smooth Particle Mesh Ewald Method. *Journal of Chemical Physics* **1995,** *103* (19), 8577-8593.
60. Wu, C.; Shea, J.-E., Structural similarities and differences between amyloidogenic and non-amyloidogenic islet amyloid polypeptide (IAPP) sequences and implications for the dual physiological and pathological activities of these peptides. *Plos Comput Biol* **2013,** *9* (8), e1003211.
61. van Gunsteren, W. F.; Weiner, P. K.; Wilkinson, T., *Computer simulation of biomolecular systems*. Published under the KLUWER/ESCOM imprint by Kluwer Academic Publishers: Dordrecht ; Boston, 1997; p 618.
62. Hanwell, M. D.; Curtis, D. E.; Lonie, D. C.; Vandermeersch, T.; Zurek, E.; Hutchison, G. R., Avogadro: an advanced semantic chemical editor, visualization, and analysis platform. *J Cheminformatics* **2012,** *4*.
63. Berendsen, H. J. C.; Postma, J. P. M.; Vangunsteren, W. F.; Dinola, A.; Haak, J. R., Molecular-Dynamics with Coupling to an External Bath. *Journal of Chemical Physics* **1984,** *81* (8), 3684-3690.
64. Hoover, W. G., Canonical dynamics: Equilibrium phase-space distributions. *Phys Rev A* **1985,** *31* (3), 1695-1697.

65. Hess, B.; Bekker, H.; Berendsen, H. J. C.; Fraaije, J. G. E. M., LINCS: A linear constraint solver for molecular simulations. *Journal of Computational Chemistry* **1997,** *18* (12), 1463-1472.
66. Miyamoto, S.; Kollman, P. A., Settle - an Analytical Version of the Shake and Rattle Algorithm for Rigid Water Models. *Journal of Computational Chemistry* **1992,** *13* (8), 952-962.
67. Towns, J.; Cockerill, T.; Dahan, M.; Foster, I.; Gaither, K.; Grimshaw, A.; Hazlewood, V.; Lathrop, S.; Lifka, D.; Peterson, G. D.; Roskies, R.; Scott, J. R.; Wilkins-Diehr, N., XSEDE: Accelerating Scientific Discovery. *Comput Sci Eng* **2014,** *16* (5), 62-74.
68. Daura, X.; Suter, R.; van Gunsteren, W. F., Validation of molecular simulation by comparison with experiment: Rotational reorientation of tryptophan in water. *Journal of Chemical Physics* **1999,** *110* (6), 3049-3055.
69. Kabsch, W.; Sander, C., Dictionary of protein secondary structure: Pattern recognition of hydrogen-bonded and geometrical features. *Biopolymers* **1983,** *22* (12), 2577-2637.
70. Touw, W. G.; Baakman, C.; Black, J.; te Beek, T. A H.; Krieger, E.; Joosten, R. P.; Vriend, G., A series of PDB-related databanks for everyday needs. *Nucleic Acids Research* **2015,** *43* (Database issue), D364-D368.

TABLE OF CONTENTS (TOC) GRAPHIC